Z. Phys. C - Particles and Fields 28, 343-356 (1985)

Zeitschrift für Physik C Particles and Fields

A Study of Photon Production in Hadronic e^+e^- Annihilation

JADE Collaboration

W. Bartel, L. Becker, D. Cords[1], R. Felst, D. Haidt, H. Junge[2], G. Knies, H. Krehbiel, P. Laurikainen[3], R. Meinke, B. Naroska, J. Olsson, D. Schmidt[2], P. Steffen[4]

Deutsches Elektronen-Synchrotron DESY, D-2000 Hamburg, Federal Republic of Germany

G. Dietrich, J. Hagemann, G. Heinzelmann, H. Kado, K. Kawagoe[5], C. Kleinwort, M. Kuhlen, K. Meier[4], A. Petersen[1], R. Ramcke, U. Schneekloth, G. Weber

II. Institut für Experimentalphysik der Universität, D-2000 Hamburg, Federal Republic of Germany

K. Ambrus, S. Bethke, A. Dieckmann, E. Elsen, J. Heintze, K.H. Hellenbrand, S. Komamiya, J. von Krogh, P. Lennert, H. Matsumura, H. Rieseberg, J. Spitzer, A. Wagner

Physikalisches Institut der Universität, D-6900 Heidelberg, Federal Republic of Germany

C. Bowdery, A. Finch, F. Foster, G. Hughes, T. Nozaki[6], J. Nye

University, Lancaster LA1 4YB, England

J. Allison, A.H. Ball, R.J. Barlow, J. Chrin, I.P. Duerdoth, T. Greenshaw, P. Hill, F.K. Loebinger, A.A. Macbeth, H.E. Mills, P.G. Murphy, K. Stephens, P. Warming

University, Manchester M13 9PL, England

R.G. Glasser, B. Sechi-Zorn[7], J.A.J. Skard, S.R. Wagner, G.T. Zorn

University of Maryland, College Park, MD20742, USA

S.L. Cartwright, D. Clarke, R. Marshall, R.P. Middleton, J.B. Whittaker

Rutherford Appleton Laboratory, Chilton, Oxon OX11 0QX, England

T. Kawamoto, T. Kobayashi, T. Mashimo, M. Minowa, H. Takeda, T. Takeshita, S. Yamada

International Center for Elementary Particle Physics, University of Tokyo, Japan

Received 3 April 1985

Abstract. The production of photons in $e^+e^- \to \gamma$ + hadrons is investigated at three centre of mass energies around 14, 22 and 34 GeV. On average, photons carry 25% of the total available energy, with a multiplicity similar to the charged multiplicity. The inclusive photon spectra are found to scale with the centre of mass energy as a function of the Feynman variable x. π^0 and η mesons are reconstructed from their decay photons. The slopes of the spectra are similar to that for charged pions and approximate scaling is observed for π^0 production. The mean π^0 and η multiplicities are given. The observed photon yield can be fully accounted for by hadron decays and initial state radiation. However, up to one extra photon per event from other sources cannot be excluded.

1 Now at SLAC, California, USA
2 Universität-Gesamthochschule Wuppertal, FRG
3 University of Helsinki, Helsinki, Finland
4 Now at CERN, Geneva, Switzerland
5 DAAD fellow
6 Now at KEK, Ibaraki, Japan
7 Deceased

1. Introduction

The production of hadrons through the annihilation of energetic electrons and positrons is described as a

process in which pointlike quark-antiquark pairs occasionally together with energetic bremsstrahlung gluons are produced initially. These partons then fragment into hadrons. In this type of reaction final state photons have the special feature that they can result from the decays of unstable hadrons or from radiative emission by either the incoming $e^{\pm}$ or the primary quarks. Quark bremsstrahlung in the quark gluon cascade is also a possible source of photons. Photons from this process could give insight into the fragmentation mechanism, provided they can be identified.

The present paper is concerned with a study of inclusive γ spectra as well as inclusive spectra of π^0 and η mesons which are identified by their two gamma decay modes. Furthermore we investigate the origin of the observed photons. The data for this analysis were taken with the JADE detector at PETRA at centre of mass energies of 14 GeV, 22.5 GeV and in the range between 29.9 and 38.7 GeV, with an average of $\sqrt{s}=34.4$ GeV. The numbers of hadronic events recorded at the three energies were 2,968, 2,353 and 23,926, respectively.

The detector, the trigger system and the event selection criteria are described in previous publications [1]. In Sect. 2 we refer only to those parts of the detector which are relevant for the present analysis, while most of this section is devoted to a description of two methods for reconstructing photons in the JADE detector. JADE offers the possibility of using either energy clusters in the lead glass arrays or the track information of e^+e^- pairs resulting from photons which converted in the material surrounding the interaction point. Inclusive photon spectra as well as π^0 and η spectra are discussed in Sect. 3, while Sect. 4 contains an investigation of photon sources and a summary of the results.

2. Photon Detection in JADE

The central tracking device of the JADE detector is a drift chamber of the jet chamber type operating in a pressurized Argon-Methane mixture at 4 bar [2]. The walls of the beam pipe and the pressure vessel present a thickness of 0.16 radiation lengths to a particle emerging from the interaction point at an angle of 90° with respect to the beam direction. The electromagnetic shower detector surrounds the tracking chamber being mounted behind the magnet coil. It consists of an array of 2,712 lead glass blocks covering polar angles of $|\cos\Theta|<0.84$ (barrel) and $0.89\leqq|\cos\Theta|\leqq0.98$ (end caps). The material preceeding the lead glass amounts to about one radiation length. After correcting for conversions and energy losses in the material in front of the lead glass, an energy resolution for photons of $\sigma(E)/E=0.04/\sqrt{E(\mathrm{GeV})}+0.015$ is achieved in the barrel part of the detector for photon energies relevant to this paper.

a) Photon Detection in the Lead Glass Arrays

Photons which do not convert in the material in front of the tracking chamber are recognized by the energy deposit in clusters of neighbouring lead glass blocks. A simple definition demands an energy exceeding 45 MeV in at least one of the blocks belonging to a cluster and requires the cluster not to be connected with a charged particle track in the central drift chamber. Such a crude definition does not distinguish between single photons, two or more photons with overlapping showers, or energy deposited by hadrons. In order to single out genuine photons in a multi-particle environment, a three dimensional shower profile is fitted to each cluster assuming that the observed energy deposit is due to a single gamma ray emerging from the principal event vertex. The free parameters of the fit are the coordinates of the impact point of the photon on the surface of the lead glass counters, while the photon energy is set to the cluster energy. The shower profile itself is described by an energy dependent parameterisation of the longitudinal development of an electromagnetic cascade in lead glass (SF5) and an energy independent lateral shape of the shower, as suggested in [3].

The photon energy is calculated by summing over all blocks belonging to a cluster correcting for energy losses in the material in front of the lead glass. For photon energies above 10 GeV the electromagnetic shower may extend into the thin glass light guides which are placed between the lead glass and the photomultiplier cathode. In these cases corrections are applied to account for the additional Cerenkov light produced in the light guides.

A comparison between the expected energy deposition in a particular block of the cluster and the observed energy allows a χ^2 function to be defined:

$$\chi^2=\sum_{i=1}^{n_b}\frac{(E_{\mathrm{cl}}f_i-E_i^{\mathrm{obs}})^2}{\sigma_i^2}$$

where the sum extends over all blocks in a cluster. E_{cl} is the observed cluster energy, f_i is the energy fraction expected in block i, while E_i^{obs} denotes the observed block energy, σ_i corresponds to the error attributed to the energy measurement in block i. The value of χ^2 can be used to distinguish between neutral clusters from single photons and clusters of other origin.

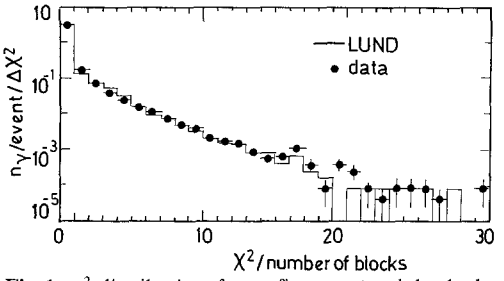

Fig. 1. χ^2-distribution for a fit to neutral lead glass clusters in multi-hadron events comparing data and a Monte Carlo simulation

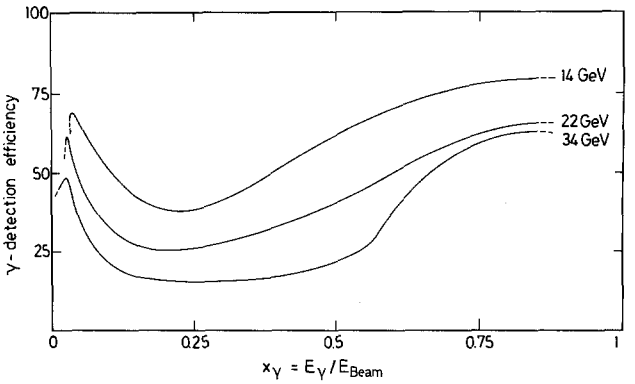

Fig. 2. Photon detection efficiency as a function of photon energy at three centre of mass energies

The validity of the reconstruction procedure has been tested by comparing experimentally observed cluster shapes with a Monte Carlo simulation of the experiment in which the Lund four vector generator [4] including initial state radiation [5] was used to create hadronic final states in e^+e^- annihilation. The generated particles were then tracked through the detector simulating all known features of the apparatus. Electromagnetic showers in the lead glass arrays were calculated with the help of the Monte Carlo code of [3], while hadronic showers were modelled according to an experimentally observed energy deposition pattern from an exposure of a small array of blocks to a pion beam with momenta between 0.5 and 3.5 GeV/c [6]. In Fig. 1 we compare the expected and observed distribution of the variable χ^2 for neutral energy clusters, normalized to the number of blocks within the cluster. The agreement is good and cuts on the quantity χ^2 are reproduced well enough by the simulation programs to be used for efficiency calculations.

From Monte Carlo studies we infer that for a cut at $\chi^2/\mathrm{DOF}<3$, this method yields an average angular resolution of $\sigma_\Theta \approx \sigma_\phi \approx 20$ mrad for photon energies around 1 GeV. At lower energies the resolution deteriorates because the number of blocks belonging to the corresponding cluster decreases with photon energy and the block structure dominates the resolution. These numbers are comparable to the resolution obtained for electrons from Bhabha scattering of $\sigma_\Theta = 10.5$ mrad and $\sigma_\phi = 12.2$ mrad [7].

The fitting algorithm for reconstructing photon directions was tested with Bhabha events by comparing the vector momenta obtained from a fit to the lead glass clusters with the directions measured in the central tracking chamber. The two methods give results which agree within the experimental errors. The energy calibration of the lead glass system is adjusted as to reproduce the beam energy in Bhabha scattering events, but there is only an indirect test of the energy assignment to low energy photons by comparing the experimentally observed π^0 mass of $m_{\pi^0} = 135 \pm 0.5$ MeV with its table value (see Fig. 11). The good agreement indicates that the photon energies are properly taken into account. Also the width of the π^0 signal $\sigma_m = 17.1 \pm 0.6$ MeV/c^2 agrees with the expectation which supports the correctness of the errors assigned to the measured quantities.

The efficiency for observing a photon in multihadron events in the JADE detector depends on the spatial density distribution of the final state particles, the read out thresholds and on parameters in the reconstruction algorithm, like cuts in the quantity χ^2, which allow us to adjust the cleanness of the photon sample. In previous publications [8] we have shown that the string model of Andersson et al. [4] reproduces the observed particle distributions. The model also describes the inclusive photon spectra which are shown in Sect. 3. Thus for efficiency calculations the model of [4] is adopted. Typical efficiency curves for reconstructing photons from neutral energy clusters in the lead glass system are shown in Fig. 2.

The shape of the efficiency curves reflects the phenomenology of hadron production through e^+e^- annihilation. Low energy photons are only weakly correlated with the jet axis. They are emitted more isotropically and are thus less affected by an overlap with other particles and their detection efficiency is high. At intermediate energy photons appear preferentially inside jets and the reconstruction efficiency is low due to overlap problems. At the upper end of the photon spectrum radiative photons dominate which are isolated and the detection probability increases. The decrease of the reconstruction efficiency with increasing centre of mass energy can be attributed to the rising multiplicity and the tighter

Table 1. Sources of background to photons observed in lead glass

	14 GeV n_γ^{fake}/evt	22 GeV n_γ^{fake}/evt	34 GeV n_γ^{fake}/evt
Neutral hadrons (K_L^0, n)	0.30	0.40	0.60
Spread out hadronic showers	0.13	0.16	0.19
Charged clusters (no track)	0.10	0.12	0.15

collimation of the hadron jets. Both items are responsible for an increasing probability of overlap with other particles.

Three sources of misidentified photons have been considered. The fraction of neutral hadrons, (K_L^0 and n) interacting in the lead glass and simulating a photon has been estimated from the known K_S^0 [9] and proton spectra [10]. Nuclear reactions of charged hadrons sometimes produce configurations which the cluster finding algorithm splits into two or more clusters. Not all of these are connected to the charged particle track and thus some are treated as photon candidates. The probability for such a confusion to occur is estimated from the observed cluster shapes in the pion beam exposure of a test module. The third source of faked photons is due to tracks which are badly reconstructed in the central chamber and fail to extrapolate to the corresponding lead glass cluster. This type of background has been estimated from a visual scan of hadronic events. These effects together may fake up to 0.9 photons per event at 34 GeV centre of mass energy and up to 0.5 at 14 GeV, as summarised in Table 1. About 0.1 photons per event may be faked by nuclear interactions in the beam pipe or in the wall of the inner detector pressure vessel, which have a π^0 in the final state. These photons are mainly of low energy and their contribution to the photon spectrum above 200 MeV has been neglegted.

Photons may be lost due to gaps between individual lead glass blocks which are not simulated in the Monte Carlo programs or by dead counters. The total loss rate due to these effects is independent of energy and amounts to 3%.

Additional systematic errors of $\pm 5\%$ affect the low energy part of the photon spectrum between 100 and 300 MeV due to uncertainties in the energy dependent acceptance. The photon spectrum above 2,500 MeV is distorted by overlapping photons from energetic π^0's, introducing an error of $\pm 8\%$ on the number of single photons. The low energy part of the inclusive photon spectrum is more affected by backgrounds than the intermediate energy regime. Thus for investigations of properties of the inclusive photon spectrum photons below 200 MeV have been ignored, while for the reconstruction of π^0 and η mesons the threshold has been lowered to 100 MeV, because faked photons contribute mainly to the combinatorial background and not to the signal.

b) Photon Detection by a Pair Spectrometer Approach

The second method of observing photons in the JADE detector employs the material between the interaction point and the sensitive elements of the central tracking chamber as a converter target allowing a photon to be reconstructed from the measured e^+e^- tracks.

The converting material consists mainly of aluminium from the beam pipe at a radius of 12.3 cm and the inner wall of the pressure vessel at a radius of 16.5 cm. In the 4 cm gap between the two tubes there is the plastic scintillator of the beam pipe counters and a thermal insulation wrapped around the beam pipe. Thus a total thickness of 16% of a radiation length with a corresponding conversion probability of about 12% has to be traversed by a photon emerging from the interaction point at 90° with respect to the beam direction.

Candidate photon conversion points are reconstructed from two oppositely charged tracks in the central detector which extrapolate, within 3σ of the measurement errors, to a common vertex inside the material surrounding the interaction point or inside the drift chamber. In order to distinguish photon conversions from secondary interactions, decays of long-lived particles, or vertices faked by nearby particles, two additional constraints were imposed. The vector sum of the two particles comprising a secondary vertex has to point to the event vertex within errors and the invariant mass of the pair has to be less than about 30 MeV (slightly depending on the track momenta).

All pairs passing the latter two cuts are treated as converted photons. In order to improve the momentum resolution a fit is made by constaining the origin of the photon to the event vertex and forcing the invariant mass of the electron positron pair to zero. The energy resolution of reconstructed photons after the constrained fit is determined mainly by the momentum resolution of the detector and by bremsstrahlung losses of the conversion electrons in the converter itself, for which only global corrections can be applied. The expected energy resolution for photons reconstructed from e^+e^- pairs and photons observed in the lead glass arrays is compared in Fig. 3. It is observed that for energies below about 700 MeV the energy resolution of the pair spectrometer approach is superior to a measurement in the lead glass array, although in the former case the

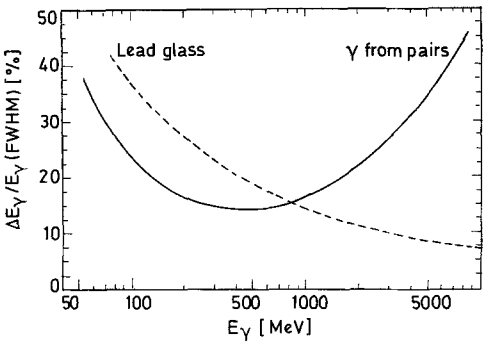

Fig. 3. Energy resolution for lead glass photons and photons reconstructed from e^+e^- pairs

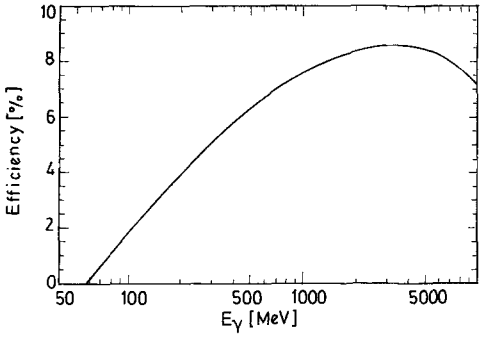

Fig. 4. Reconstruction efficiency for photons seen as e^+e^- pairs

resolution deteriorates with decreasing energy because of multiple scattering.

As in the case of photons observed in the lead glass arrays, the reconstruction efficiency shown in Fig. 4 was calculated with the help of Monte Carlo programs. The efficiency quickly deteriorates for photon energies below 200 MeV because the pattern recognition probability for track finding below 50 MeV is reduced. In addition low energy tracks are contaminated with secondary particles emerging from the walls of the beam pipe as well as by knock on electrons and only after severe cuts can they be used for reconstructing secondary vertices. The detection efficiency contains an uncertainty of about $\pm 6\%$, resulting from the error on the converter thickness introduced by measurement errors on the production angle Θ. An additional systematic error of $\pm 12\%$ takes into account deficiencies of the Monte Carlo simulation of converted photons in the JADE detector, especially for the simulation of electron tracks below about 100 MeV.

The background contamination in the γ-sample reconstructed by the pair spectrometer method is on the average 10% mainly due to misidentified hadronic interactions. In estimating this number the observed mass spectrum associated with conversion pairs has been extrapolated into the region of the mass cut i.e. below 30 MeV. Another input to the background estimate employed a measurement of the specific ionisation of the particles emerging from the conversion vertex. Such a dE/dx measurement applies only to a restricted sample with especially well measured tracks. In this sample the background contamination is only of the order of 5%.

The validity of the pair spectrometer approach and the error estimates have been tested by comparing the observed position and width of the π^0 signal reconstructed from converted photons with Monte Carlo predictions. Also here the agreement is satisfactory.

The two independent methods of detecting photons with JADE by a) observing neutral energy clusters in the lead glass arrays and b) using the detector as a pair spectrometer are complementary to the extent that at energies below 700 MeV the latter approach provides the better momentum resolution. Furthermore both methods have different systematic errors and thus allow for cross checks.

3. Inclusive Spectra

The investigation of inclusive momentum distributions of charged particles as well as of photons in e^+e^- annihilation events is important for understanding the fragmentation of quarks and gluons into hadrons. But not all photons are of hadronic origin and at energies exceeding about half the beam energy a substantial contribution to the photon yield can be attributed to initial state radiation of the incoming electron and positron. For a physics analysis, however, these two sources of photons have to be separated.

a) Inclusive Photon Spectra

For the analysis of inclusive photon production we consider only photons with energies above 200 MeV in order to keep the background low. The photon spectrum at 34 GeV centre of mass energy after acceptance corrections is shown in Fig. 5, together with the expectation of the Lund model and a calculation of initial state radiation according to [5]. In general the model reproduces the measured data well except that in the range of $0.2 < x < 0.3$ the data lie systematically below the model prediction. This discrepancy is, however, small and does not affect efficiency calculations which use the Lund four vector generator. Above $x = 0.5$ the photon spectrum is dominated by radiative photons and the agreement between prediction and observation is reasonable. It supports the correctness of the approximations made to calculate the high energy part of the radiative corrections.

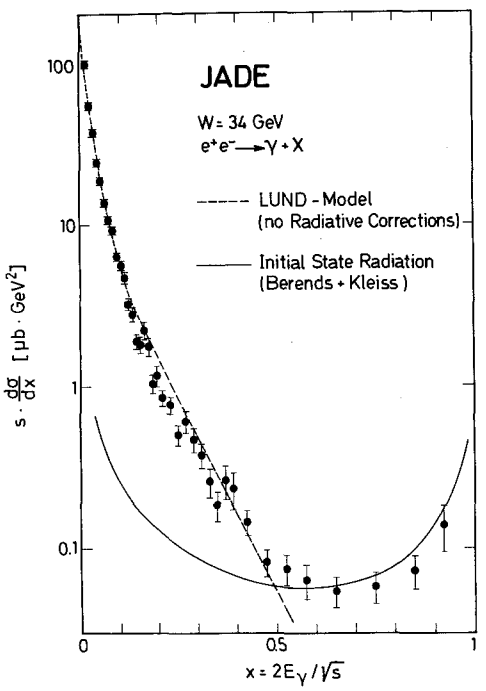

Fig. 5. Photon spectrum at 34 GeV centre of mass energy before radiative correction

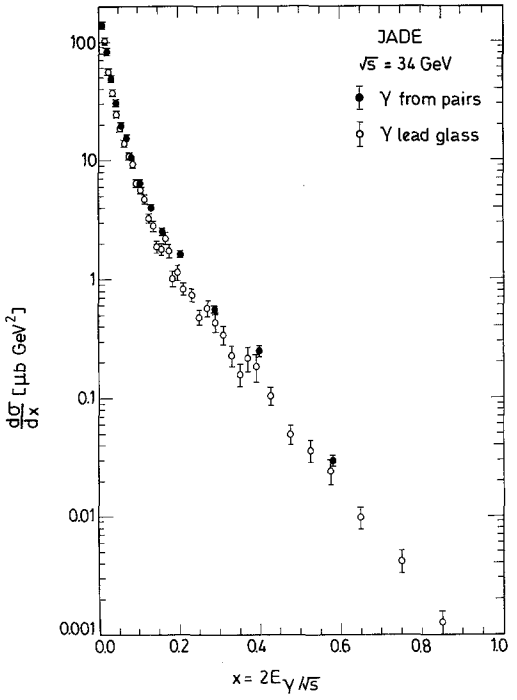

Fig. 6. Comparison of photon spectra from lead glass photons and photons reconstructed from pairs at 34 GeV centre of mass energy

A statistically significant comparison of the spectra obtained from photons recorded in the lead glass and from photons which are reconstructed from pairs is only possible using the large data sample at 34 GeV. The result of the comparison is shown in Fig. 6, where the photon yields after acceptance corrections and radiative corrections are displayed as a function of the normalized photon energy. The errors in this plot are statistical only. Within these errors both spectra agree, although the data points from lead glass photons lie systematically below those derived from pairs by about 15%. This difference which is within the quoted systematic errors is probably due to an underestimate of the vertex finding efficiency and of the conversion probability.

For further analysis, only photons observed in the lead glass arrays were used because of their smaller statistical and systematic errors. In Fig. 7a, b, c the inclusive photon spectra $s\frac{d\sigma}{dx}$ after acceptance corrections and radiative corrections, are shown, while Fig. 8 contains a combined plot of JADE and CELLO data [11] at centre of mass energies of 34, 22 and 14 GeV. The cross sections measured by the two experiments agree within errors and there is no indication of scaling violation. The latter statement can be quantified by evaluating the integral $\int_{0.2}^{0.5} s(d\sigma/dx)dx$ at the three centre of mass energies. We obtain 0.11 ± 0.02, 0.10 ± 0.03 and 0.13 ± 0.03 μb GeV^2 as integrated cross sections for 34, 22 and 14 GeV respectively. Assuming the Lund model as a guideline, the expected difference between the inclusive photon cross sections at 34 GeV and 14 GeV at a normalised photon energy $x = 0.5$ is less than a factor of two and is thus too small to be established by the present experiment with its limited statistical accuracy. An observation of a significant scaling violation would require higher statistics preferably at higher energy to increase the lever arm.

The photon spectra may be compared with the charged pion spectra at the same centre of mass energy. At 34 GeV we compare (Fig. 9) the photon spectrum of the present analysis with the charged pion spectrum published by TASSO [10]. The difference in slope of the two spectra is clearly visible, the photon spectrum being softer. A measure of this difference is inferred by comparing fits to the invariant cross section $E/4\pi p^2\, d\sigma/dp$, as a function of the particle energy E, to the sum of three exponentials

$$\frac{E}{4\pi p^2}\frac{d\sigma}{dp} = \sum_{m=1}^{3} A_m e^{-B_m E}.$$

Such a fit is published by the TASSO group in [10] for charged pions. The γ spectrum can also be described by a superposition of three exponentials with

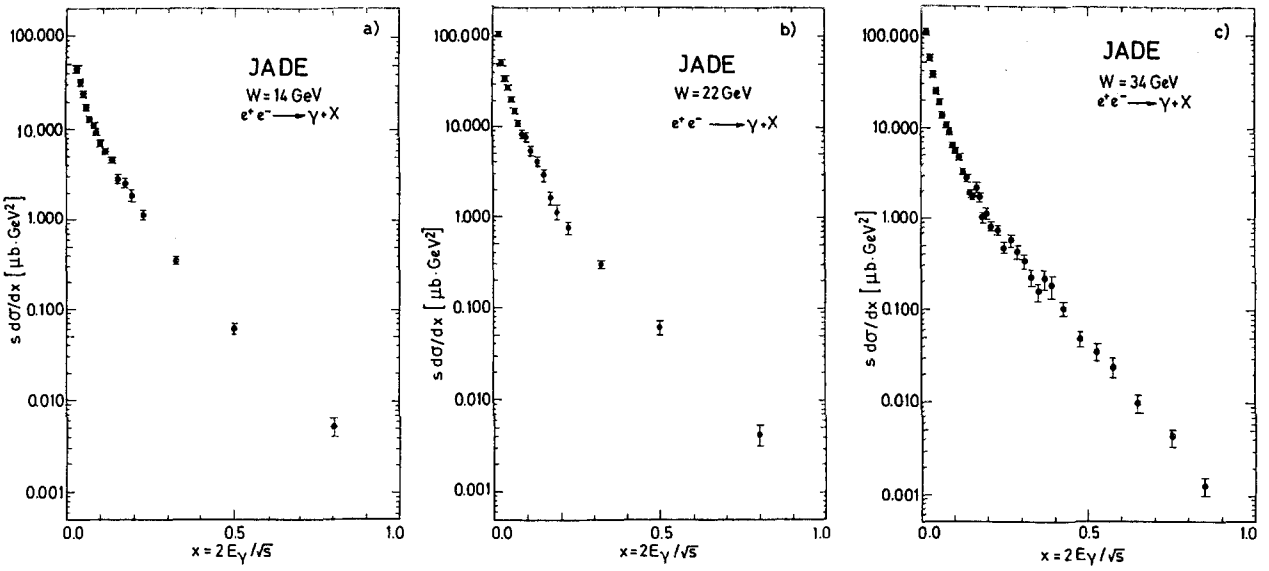

Fig. 7. Photon spectra at **a** 14 GeV, **b** 22 GeV, **c** 34 GeV centre of mass energy

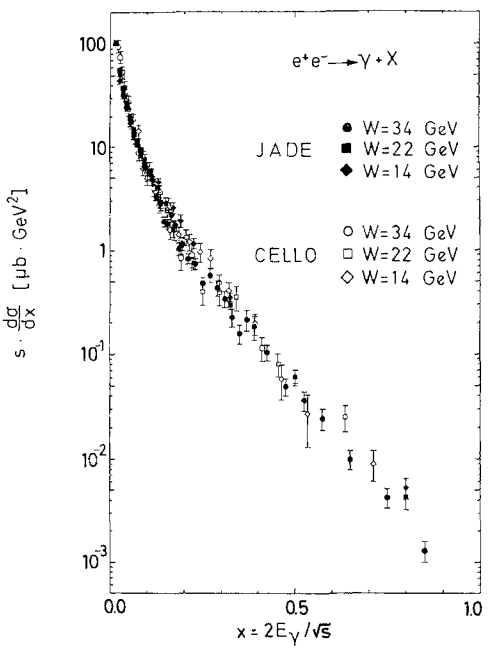

Fig. 8. Scaling cross section at three centre of mass energies

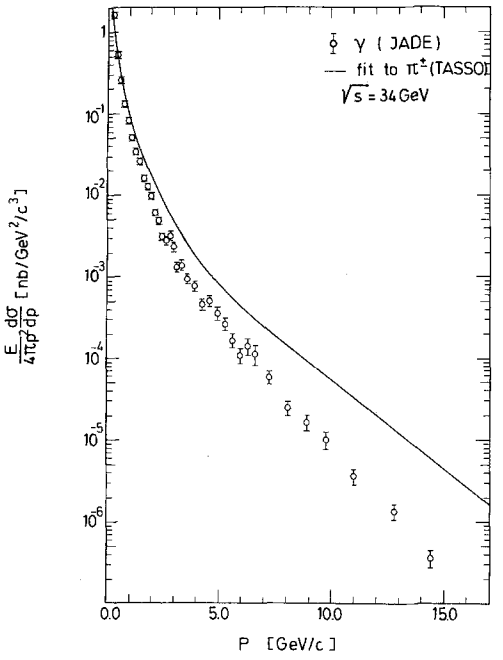

Fig. 9. Inclusive photon spectrum and a fit to the charged pion spectrum (TASSO) at 34 GeV

a χ^2 of 29 for 30 degrees of freedom. The slope parameters B_m for charged pions and photons are compared in Table 2 indicating that the photon spectrum drops about twice as fast as the pion spectrum as a function of energy, while in both cases the relative magnitude of the coefficients A_i is of the order of $A_1:A_2:A_3=1:0.1:0.001$. This observation is a consequence of the fact that the majority of the photon stems from π^0 decays. The errors on the parameters B_m quoted for the photon spectrum correspond to 68% confidence level in a 6 dimensional parameter space and include systematic effects.

The spectra at lower centre of mass energy are also well fitted by a superposition of three exponentials, while only two exponentials are insufficient for a satisfactory description of the data. Although TASSO has published only fits with two exponentials to the charged pion spectrum, the slope parameters B_1 and B_2 may be compared, because the contribution of the third exponential is small. Also here we find

Table 2. Slope parameters B_m for 34 GeV cm energy

	γ spectrum JADE	$\pi^\pm$ spectrum TASSO
B_1	7.97 ± 1.75	4.97 ± 0.45
B_2	2.34 ± 0.28	1.51 ± 0.21
B_3	0.71 ± 0.05	0.50 ± 0.08

that the slopes describing the γ spectra are two to three times larger than the corresponding parameters for the charged pion spectra.

b) Photon Multiplicity

The photon multiplicity is obtained by an integration over the entire photon spectrum.

$$\langle n_\gamma \rangle = \frac{1}{\sigma_{\text{tot}}} \int_0^1 (d\sigma_\gamma/dx)\, dx.$$

The integral extends down to $x=0.$ into an energy range which is not accessible to the experiment. The low energy part of the integral has thus been estimated with the help of the Lund model normalising the model prediction to the total number of events. The extrapolation factors vary between 1.43 at 34 GeV and 1.47 at 14 GeV and a systematic error of 10% has been attributed to the extrapolation. At 34 GeV the photon multiplicity corrected for acceptance and radiative effects is $13.7 \pm 0.4 \pm 0.7$ if only photons seen in the lead glass arrays are used and $15.5 \pm 0.6 \pm 1.1$ for photons which are reconstructed from pairs. The photon multiplicities together with the fractions of other particles are summarised in Table 3. It is observed that the photon multiplicity increases at the same rate as the pion or total charged multiplicity with increasing centre of mass energy, and photons appear to be as abundant as charged particles.

c) Energy Fraction Carried by Photons

The average energy fraction carried by photons in hadronic events is computed by integrating the photon spectrum weighted with the normalised γ momentum x.

$$\langle \rho_\gamma \rangle = \frac{1}{2\sigma_{\text{tot}}} \int_0^1 x(d\sigma_\gamma/dx)\, dx.$$

Also here the Lund model has been used to estimate the contribution to the integral in the region not accessible to the experiment. The measured photon energy fractions are summarised in Table 4. In a previous publication [13] a calorimetric method was described to assess ρ_γ, in which the photon energy was calculated from the total observed energy in the lead glass system by subtracting the energy deposit due to hadrons. Because of systematic errors in the hadronic energy deposition this method is less accurate than a direct computation from the measured photon spectrum. Both methods which are independent of each other give consistent results within errors.

Comparing the present data with previous measurements [13, 14] leads to the conclusion that the photon energy fraction is about 1/4 of the total energy available and is constant between 5 GeV and 34 GeV which may be read off Fig. 10.

d) π^0 Spectra

In forming all two-photon mass combinations for photons with energies above 0.1 GeV, a plot of the invariant masses versus the number of combinations exhibits a peak at the position of the π^0 mass with $m_{\pi^0} = 135 \pm 0.5\ \text{MeV/c}^2$ and width $\sigma_m = 17.1 \pm 0.6\ \text{MeV/c}^2$ above a smooth background as shown in Fig. 11. The π^0 yield is deduced from the observed two photon mass spectrum by fitting a polynomial background plus a Gaussian resolution function to the data points. The detection efficiency for π^0's at the three centre of mass energies is displayed in Fig. 12 as a function of the π^0 momentum. The loss of efficiency above 1.5 GeV/c can be attributed to the block structure of the counter array, whereas at low energy the acceptance drops due to the cut on the photon energy. The variation of the reconstruction probability with centre of mass energy reflects the single photon detection efficiency of Fig. 2. In-

Table 3. Particle multiplicities as a function of cm energy

Type	14 GeV	22 GeV	34 GeV	Ref.
γ	$8.5 \pm 0.6 \pm 0.5$	$11.4 \pm 0.7 \pm 0.7$	$13.7 \pm 0.4 \pm 0.7$	
π^0	$4.7 \pm 0.2 \pm 0.2$	$5.5 \pm 0.4 \pm 0.3$	$6.1 \pm 0.1 \pm 0.3$	
$\pi^+ + \pi^-$	7.2 ± 0.6	10.0 ± 0.7	10.3 ± 0.4	TASSO [10]
charg.	9.08 ± 0.05	11.22 ± 0.07	13.48 ± 0.03	TASSO [12]

Table 4. Photon energy fractions as a function of cm energy

E_{cm}(GeV)	$\langle \rho_\gamma \rangle$(%)
14	$25.1 \pm 2.1 \pm 1.4$
22	$24.9 \pm 2.2 \pm 1.4$
34	$24.3 \pm 1.7 \pm 1.6$

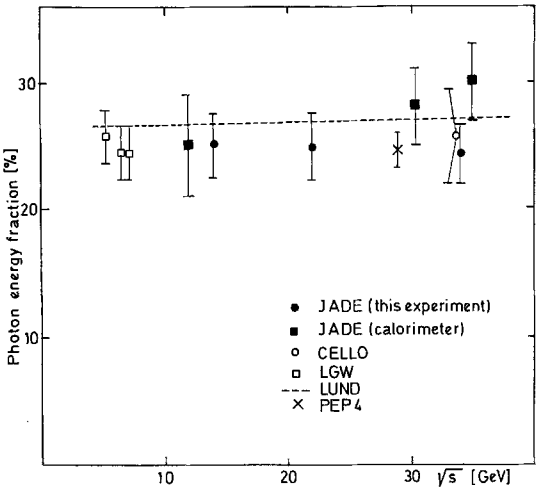

Fig. 10. Energy fraction carried by photons in hadronic annihilation events

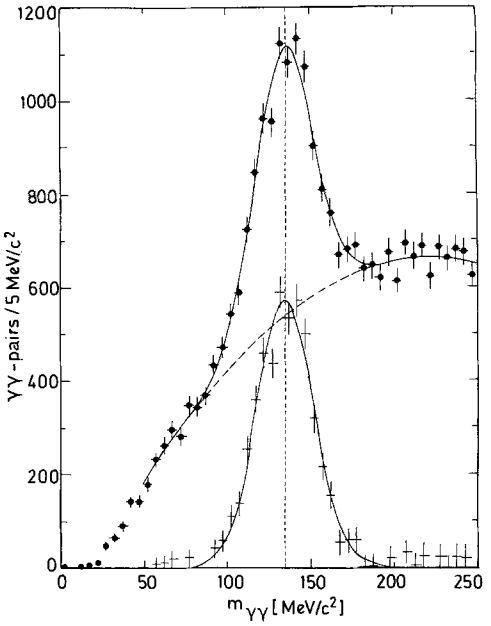

Fig. 11. Two γ invariant mass spectrum in the range of the π^0 mass with a Gaussian plus a polynomial background fitted to the data. Insert: π^0 signal after background subtraction

side jets the fraction of π^0 mesons which are found by the analysis programs is as high as 28% at 14 GeV centre of mass energy.

The scaling cross sections for inclusive π^0 production at the three centre of mass energies are

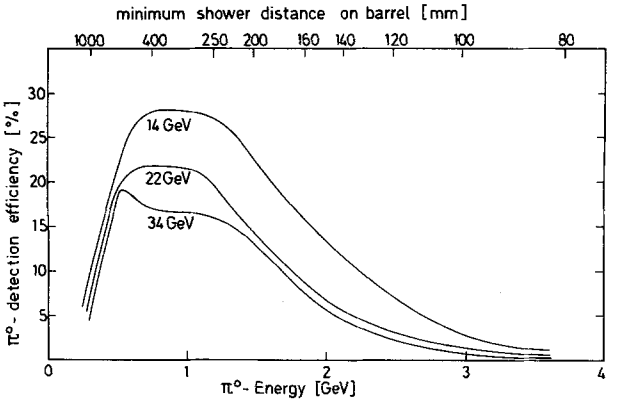

Fig. 12. Reconstruction efficiency for π^0 in hadronic annihilation events

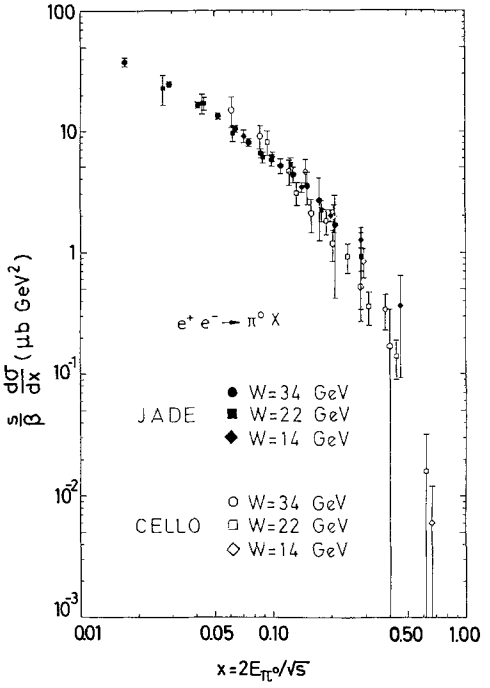

Fig. 13. Scaling cross section for π^0 production at three centre of mass energies

plotted in Fig. 13 together with previously published data of the CELLO collaboration [11]. No scaling violation is observable. Earlier data of the TASSO group [15] which are based on a considerably smaller data sample agree within errors with the cross sections of the present evaluation. A comparison with the charged pion spectrum of the TASSO group scaled by a factor of two is shown in Fig. 14. At 34 GeV the two cross sections agree with each other reasonably well in the range of overlap.

Integrating the inclusive π^0 spectra, with an extrapolation over the small energy range which is not observed in this experiment, neutral pion fractions are obtained which are listed in Table 3. They match

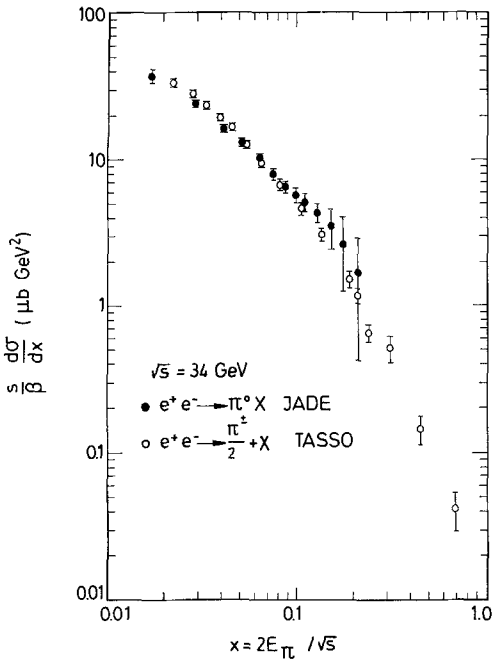

Fig. 14. π^0 and $\pi^\pm$ spectra at 34 GeV centre of mass energy

the charged pion multiplicities divided by two, as expected from the close similarity of the differential energy spectra.

e) η-Spectra

The measurement of inclusive η production through the decay $\eta \to \gamma\gamma$ at 34 GeV centre of mass energy has been described in a previous publication [16] and only the main features of the analysis will be repeated here. For the present paper the analysis has been repeated with a data sample which is 30% bigger and with efficiency calculations based on a Monte Carlo event sample which was increased by a factor of three.

An analysis of η production is only sensible with the large data sample available at 34 GeV centre of mass energy. An η signal is observed in the two photon mass spectrum after removing photons which contribute to the π^0 peak, restricting the sum of the two γ energies $E_{\gamma 1}+E_{\gamma 2}>0.7$ GeV, and requiring that both photons lie in the same hemisphere of the event. Here the event hemispheres are defined by the two sides of a plane through the event vertex which is perpendicular to the sphericity axis. The η signal is centered around $m_\eta = 575 \pm 13$ MeV/c^2 with a resolution of $\sigma_m = 64 \pm 16$ MeV/c^2, as shown in Fig 15. The cross sections for inclusive η production are given in the tables of the appendix. They agree within errors with the values given in the earlier publication although it should be noted, that the new analysis yields a cross section at $\langle x \rangle = 0.047$ which is about one standard deviation lower. By integrating the η spectrum an average number of $\langle n_\eta \rangle = 0.64 \pm 0.15$ per event is obtained. Comparing the η yield with the production of $\pi^\pm$ in Fig. 16 leads to the conclusion that the slopes of the two spectra are very similar.

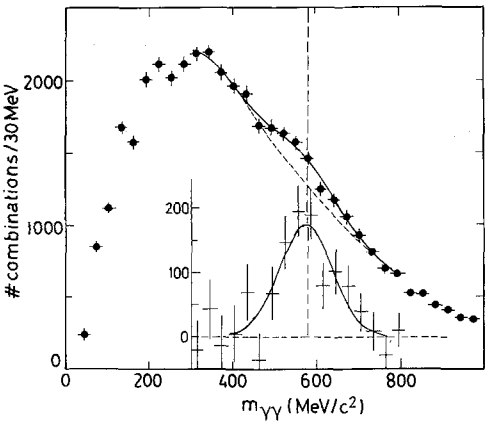

Fig. 15. Two photon invariant mass spectrum after removal of photons forming a π^0 with $E_{\gamma 1}$, $E_{\gamma 2} > 300$ MeV. Insert: η signal after background subtraction

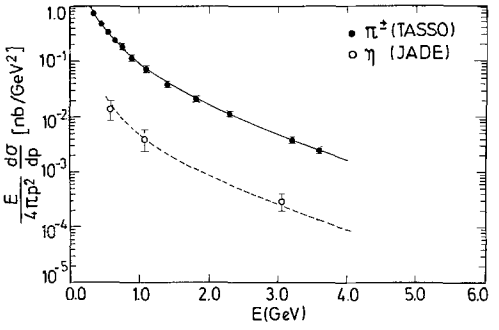

Fig. 16. Inclusive η production rate and inclusive $\pi^\pm$ cross section. The curves are a TASSO fit to the $\pi^\pm$ spectrum and the same fit scaled down drawn through the η points

In the paper of [16] an attempt was made to relate the η abundance to the emission of energetic gluons. Although the η fraction seems to rise more rapidly with increasing event sphericity than the π^0 fraction, no statistically significant signal has been observed for an enhancement of the η yield in planar or spherical events. The increase in statistics for the present analysis is not sufficient to go beyond the previous conclusions.

4. A Study of Photon Sources

As already mentioned in the previous chapter, the majority of photons are associated with π^0 decays. A quantitative evaluation of the known γ sources and a comparison with the observed photon spectrum allows limits to be set on new sources.

a) New Particle Search in $e^+e^- \to \gamma + X$

The photon spectra of Fig. 7 do not exhibit any obvious structure which could be attributed to monoenergetic photon lines. These may result from reactions of the type $e^+e^- \to \gamma + X$, where X is a neutral particle of mass m_x. In order to set limits on the presence of gamma lines the spectra $E/(4\pi p^2) \cdot d\sigma/dp$ have been fitted to a superposition of three exponentials as described in Sect. 3. The residuals were then fitted to Gaussians with an energy dependent width corresponding to the observed photon energy resolution. None of the Gaussians was statistically significant and upper limits are given for the production of X-particles. The photon detection efficiency was assumed to be the same as in multi-hadron events, which is conservative especially in the case of X being a scalar or pseudo scalar where the efficiency should be higher. The maximum Gaussian which is compatible with the data at 14 GeV occurs at a photon energy of $E_\gamma = 1.05$ GeV corresponding to a mass $m_x = 12.9$ GeV with a cross section of $\sigma < 8.6 \cdot 10^{-2}$ nb at 95% C.L. At 22 GeV the maximum occurs at $E_\gamma = 3.7$ GeV corresponding to $m_x = 17.9$ GeV with $\sigma < 3.2 \cdot 10^{-3}$ nb at 95% confidence level. The 34 GeV data sample which consists of events taken at various centre of mass energies has a major input at $E_{cm} = 34.6$ GeV. At this energy a maximum of $\sigma < 2.7 \cdot 10^{-3}$ nb is obtained at $E_\gamma = 5.9$ GeV corresponding to $m_x = 28.0$ GeV. This analysis does not show evidence for the production of a new particle especially a scalar X. Furthermore the mass values at which the maximum Gaussians occur are not correlated.

b) Photon Sources

In order to study the sources which contribute to the observed photon spectrum in more detail, the γ spectrum due to π^0 and η decays has been computed by folding the measured π^0 and η spectra with the appropriate decay kinematics. From Fig. 17, where we compare the measured photon spectrum with the one originating from π^0 and η decays, it is inferred that almost all photons can be attributed to these sources.

A limit on the number of photons not accounted for by known decay processes is obtained by subtracting the number of photons due to π^0 and η decays from the measured photon multiplicity. The remainder, which is listed in Column 2 of Table 5, still contains photons from hadron decays as there are ω, η' and charm decays. We have used the Lund model to estimate their contribution. The residual photon multiplicity which appears in the last column of Table 5 is compatible with zero. Due to experimental and theoretical uncertainties there could be room for at most one additional photon per event from other sources.

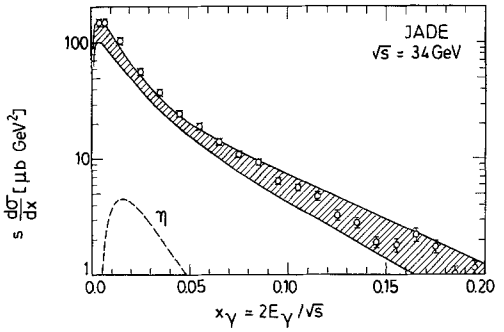

Fig. 17. Photon spectrum reconstructed from π^0 and η production. The hatched area reflects the experimental uncertainty in reconstrucing the γ-spectrum from measured π^0 and η spectra

Table 5. Origin of Photons. $\#\gamma$ per event after subtracting known γ sources

E_{cm}	Remove $\pi_0, \eta \to \gamma\gamma$	Remove hadron decays into γ
34	0.55 ± 1.1	0.35 ± 1.1
22	0.35 ± 1.1	0.15 ± 1.1
14	-0.87 ± 1.0	-1.00 ± 1.0

c) Direct Photons from Quark Bremsstrahlung

One photon source of interest is related to the emission of bremsstrahlung photons by quarks. In this case, bremsstrahlung emission is competing with the quark fragmentation, and the γ spectrum could serve as a probe for quark momentum distributions in the quark gluon cascade. These photons are difficult to isolate experimentally, because they are mixed with photons from initial state radiation or decay processes. In an angular region far from the beam line and the jet axis, high energy photons from quark bremsstrahlung might possibly be observed [17].

We have looked for a signal of bremsstrahlung photons off primary quarks at 34 GeV centre of mass energy by selecting isolated photons, with no other particle in a cone with a half opening angle of 20°, a transverse momentum with respect to the jet axes of $p_T \geqq 2$ GeV, and an energy between 2 and 8 GeV. In order to reduce the contribution from initial state radiation, the angle with respect to the beam direction was required to exceed 40.5°. After subtracting the number of photons expected from initial state radiation and hadron decays, we are left with a small excess of 56 ± 22 photons. The kinematic region is chosen such that QCD corrections [17] to

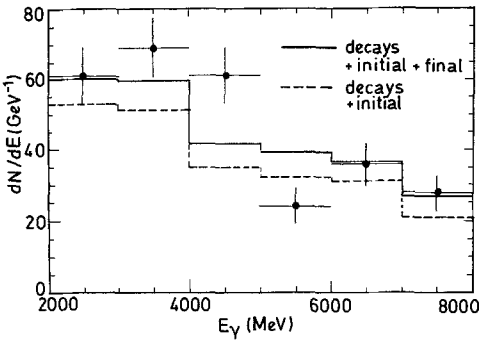

Fig. 18. Photon spectrum after cuts described in the text to enrich quark bremsstrahlung photons

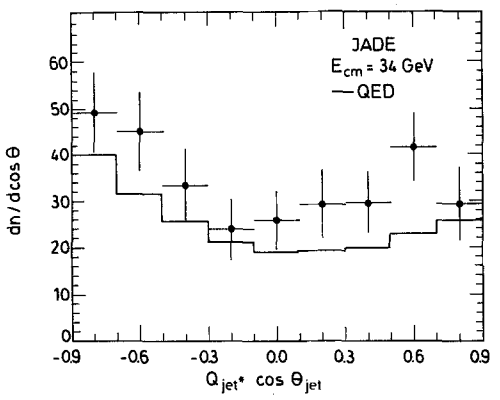

Fig. 19. $\cos\Theta$ of the jet axis w.r.t. the beam multiplied with the sign of the reconstructed quark charge for events of the quark bremsstrahlung enriched sample. The QED labelled curve is an adaptation of the $\mu\mu\gamma$ cross section to quarks

the direct photon emission are small and bremsstrahlung by the primary quarks dominates. Thus the observed number of photons can be compared to an estimate of 41 ± 5, which is based on an adaptation to fractionally charged quarks of the QED order $\alpha^3 \mu^+ \mu^- \gamma$ cross section given by Berends and Kleiss in [18].

The photon energy spectrum for all the photons which pass the above cuts is shown in Fig. 18. The dashed line shows the expectation for initial state radiation and hadron decays only; the solid line is this contribution plus that from the final state radiation and interference terms. It should be noted that 12 out of the 279 photons in Fig. 18 come from events where two photons pass all of the cuts. The Monte Carlo studies which only include QED up to order α^3 indicate that we should not see any event with two photons which pass our cuts, so these 6 events with two high p_T isolated photons are possible evidence for the QED order α^4 process $e^+e^- \to q\bar{q}\gamma\gamma$.

In addition to increasing the number of photons observed in e^+e^- annihilations, final state radiation should also induce a charge asymmetry at the quark production level, due to interference between initial and final state radiation [19]. If one can determine the signs of the initial quark charges from their fragmentation products, it should be possible to measure this asymmetry with a large enough data sample. We enhanced final state radiation photons by using the cuts described in the previous paragraph, and used a standard method of assigning charges to jets. This method, which was also used by the MAC experiment [20] for their study of this interference effect, was to sum up all charges in a jet for tracks with $p > 250$ MeV and assign the sign of the sum to the sign of the parent quark charge. We plot the quark charge sign times $\cos\Theta$ of the jet for $|\cos\Theta| \leqq 0.9$ in Fig. 19. After subtraction of the decay contributions calculated by Monte Carlo programs, an average asymmetry $\bar{A} = -0.06 \pm 0.07$ remains. The Monte Carlo calculations on the basis of the $\alpha^3 \mu\mu\gamma$ cross section indicate that, with a probability of assigning the quark charge correctly of 0.66 ± 0.06 we should expect an asymmetry of -0.14 ± 0.05, with the largest contribution to the error of the expected asymmetry coming from the uncertainty in the quark charge assignment. The systematic differences between the data and the QED labelled angular distribution of Fig. 19 as well as the differences showing up in the energy spectrum of Fig. 18 could be due to neglecting soft radiative corrections which are estimated to be of the order of 20% according to [21]. Our measurement is consistent with zero asymmetry, but it is clear that we need a much larger data sample to confirm or refute the existence of this asymmetry.

Conclusion

At the three centre of mass energies, 14, 22 and 34 GeV inclusive gamma spectra have been measured in hadronic final states produced by e^+e^- annihilation processes. They do not exhibit any fine structure and it is found that for normalized γ energies $x = E_\gamma / E_{cm} > 0.025$ the cross section $s\, d\sigma_\gamma / dx$ is within errors independent of the centre of mass energy and no scaling violation is observed. The photon multiplicity is seen to rise at the same rate with increasing energy as the multiplicity of charged particles, and photons carry a constant fraction of about 25% of the total energy between 5 and 34 GeV centre of mass energy.

π^0 mesons have been reconstructed from their decay photons and their spectrum is found to have the same features as the charged pion spectrum, indicating that the sources for the two species are essentially the same. The mean number of π^0's per event corresponds to half the number of charged pions.

It is observed that at 34 GeV centre of mass energy η mesons are produced with an abundance of 0.64 ± 0.15 η's per hadronic event. The slope of the inclusive η spectrum is found to be similar to that for pions. No significant dependence of the η production on event shape has been found.

The majority of final state photons after subtracting initial state radiation can be attributed to π^0 decays with smaller contributions from η and other hadronic decays. Additional photons are limited to less than about one extra photon per event. In particular bremsstrahlung emission from the primary quarks has been searched. The presently available data sample does not, however, allow a statistically significant confirmation of this effect.

Acknowledgement. We are indebted to the PETRA machine group and the group of the computer centre for their excellent support during the experiment and to all the engineers and technicians of the collaborating institutions who have participated in the construction and maintenance of the apparatus. This experiment was supported by the Bundesministerium für Forschung und Technologie, by the Ministry of Education, Science and Culture of Japan, by the UK Science and Engineering Research Council through the Rutherford Appleton Laboratory and by the US Department of Energy. The visiting groups at DESY wish to thank the DESY directorate for the hospitality extended to them.

Appendix

Table A1. Inclusive γ spectrum at $\langle\sqrt{s}\rangle = 34.4$ GeV

$\langle x \rangle$	$s\,d\sigma/dx$(μb GeV^2)	$\langle x \rangle$	$s\,d\sigma/dx$(μb GeV^2)
0.015	$103.0 \pm 1.1 \pm 9.0$	0.195	$1.2 \pm 0.2 \pm 0.1$
0.025	$56.3 \pm 0.8 \pm 3.9$	0.210	$0.83 \pm 0.1 \pm 0.07$
0.035	$37.7 \pm 0.7 \pm 0.3$	0.230	$0.74 \pm 0.09 \pm 0.06$
0.045	$24.7 \pm 0.6 \pm 0.3$	0.250	$0.48 \pm 0.07 \pm 0.04$
0.055	$19.2 \pm 0.6 \pm 0.3$	0.270	$0.57 \pm 0.09 \pm 0.05$
0.065	$14.0 \pm 0.5 \pm 0.3$	0.290	$0.44 \pm 0.07 \pm 0.04$
0.075	$10.9 \pm 0.5 \pm 0.3$	0.310	$0.34 \pm 0.06 \pm 0.03$
0.085	$9.4 \pm 0.5 \pm 0.3$	0.330	$0.23 \pm 0.04 \pm 0.02$
0.095	$6.4 \pm 0.4 \pm 0.3$	0.350	$0.16 \pm 0.03 \pm 0.01$
0.105	$5.7 \pm 0.4 \pm 0.3$	0.370	$0.22 \pm 0.05 \pm 0.02$
0.115	$4.8 \pm 0.4 \pm 0.3$	0.390	$0.18 \pm 0.05 \pm 0.02$
0.125	$3.3 \pm 0.3 \pm 0.3$	0.425	$0.10 \pm 0.02 \pm 0.01$
0.135	$2.8 \pm 0.3 \pm 0.3$	0.475	$0.049 \pm 0.01 \pm 0.004$
0.145	$1.9 \pm 0.2 \pm 0.3$	0.525	$0.036 \pm 0.008 \pm 0.003$
0.155	$1.8 \pm 0.2 \pm 0.3$	0.575	$0.024 \pm 0.006 \pm 0.002$
0.165	$2.2 \pm 0.3 \pm 0.3$	0.650	$0.010 \pm 0.002 \pm 0.001$
0.175	$1.8 \pm 0.2 \pm 0.3$	0.750	$0.004 \pm 0.001 \pm 0.0004$
0.185	$1.0 \pm 0.1 \pm 0.3$	0.850	$0.0013 \pm 0.0003 \pm 0.0001$

Table A2. Inclusive γ spectrum at 22.5 GeV

$\langle x \rangle$	$s\,d\sigma/dx$(μb GeV^2)	$\langle x \rangle$	$s\,d\sigma/dx$(μb GeV^2)
0.015	$104.0 \pm 5.7 \pm 7.1$	0.110	$5.35 \pm 0.5 \pm 0.2$
0.025	$51.3 \pm 1.6 \pm 3.5$	0.130	$4.1 \pm 0.4 \pm 0.15$
0.035	$34.5 \pm 1.4 \pm 1.6$	0.150	$2.8 \pm 0.4 \pm 0.10$
0.045	$27.5 \pm 1.3 \pm 1.3$	0.170	$1.6 \pm 0.3 \pm 0.04$
0.055	$20.5 \pm 1.2 \pm 0.9$	0.190	$1.13 \pm 0.2 \pm 0.03$
0.065	$14.7 \pm 1.0 \pm 0.7$	0.225	$0.76 \pm 0.1 \pm 0.06$
0.075	$10.9 \pm 0.9 \pm 0.5$	0.325	$0.30 \pm 0.03 \pm 0.03$
0.085	$8.3 \pm 0.8 \pm 0.4$	0.5	$0.06 \pm 0.01 \pm 0.005$
0.095	$7.7 \pm 0.8 \pm 0.3$	0.8	$0.004 \pm 0.001 \pm 0.0004$

Table A3. Inclusive γ spectrum at 14 GeV

$\langle x \rangle$	$s\,d\sigma/dx$(μb GeV^2)	$\langle x \rangle$	$s\,d\sigma/dx$(μb GeV^2)
0.025	$44.6 \pm 3.7 \pm 3.0$	0.130	$4.6 \pm 0.4 \pm 0.2$
0.035	$31.7 \pm 1.2 \pm 2.2$	0.150	$2.9 \pm 0.3 \pm 0.1$
0.045	$24.0 \pm 0.9 \pm 1.0$	0.170	$2.6 \pm 0.3 \pm 0.1$
0.055	$17.2 \pm 0.9 \pm 0.8$	0.190	$1.9 \pm 0.3 \pm 0.09$
0.065	$12.8 \pm 0.7 \pm 0.6$	0.225	$1.15 \pm 0.1 \pm 0.05$
0.075	$11.0 \pm 0.7 \pm 0.5$	0.325	$0.35 \pm 0.03 \pm 0.02$
0.085	$9.35 \pm 0.7 \pm 0.4$	0.5	$0.06 \pm 0.01 \pm 0.006$
0.095	$7.0 \pm 0.6 \pm 0.3$	0.8	$0.005 \pm 0.001 \pm 0.0005$
0.11	$5.8 \pm 0.4 \pm 0.3$		

Table A4. Inclusive π^0 spectrum at $\langle\sqrt{s}\rangle = 34.4$ GeV

$\langle x \rangle$	$s/\beta\,d\sigma/dx$(μb GeV^2)	$\langle x \rangle$	$s/\beta\,d\sigma/dx$(μb GeV^2)
0.017	$37.8 \pm 3.4 \pm 8.9$	0.099	$5.77 \pm 0.66 \pm 0.26$
0.029	$24.6 \pm 1.2 \pm 2.1$	0.110	$5.16 \pm 0.73 \pm 0.18$
0.041	$16.5 \pm 1.0 \pm 1.2$	0.128	$4.35 \pm 0.65 \pm 0.32$
0.052	$13.4 \pm 0.8 \pm 0.6$	0.151	$3.51 \pm 1.06 \pm 0.15$
0.064	$10.4 \pm 0.7 \pm 0.5$	0.174	$2.66 \pm 1.42 \pm 0.30$
0.075	$8.1 \pm 0.6 \pm 0.34$	0.209	$1.67 \pm 1.25 \pm 0.30$
0.087	$6.56 \pm 0.57 \pm 0.39$		

Table A5. Inclusive π^0 spectrum at 22.5 GeV

$\langle x \rangle$	$s/\beta\,d\sigma/dx$(μb GeV^2)	$\langle x \rangle$	$s/\beta\,d\sigma/dx$(μb GeV^2)
0.027	$22.9 \pm 6.3 \pm 5.4$	0.124	$5.28 \pm 0.70 \pm 0.22$
0.044	$16.9 \pm 2.1 \pm 1.8$	0.178	$2.22 \pm 0.44 \pm 0.11$
0.062	$9.6 \pm 1.4 \pm 0.8$	0.285	$0.92 \pm 0.65 \pm 0.37$
0.089	$6.1 \pm 0.6 \pm 0.4$		

Table A6. Inclusive π^0 spectrum at 14 GeV

$\langle x \rangle$	$s/\beta\,d\sigma/dx$(μb GeV^2)	$\langle x \rangle$	$s/\beta\,d\sigma/dx$(μb GeV^2)
0.043	$17.1 \pm 3.2 \pm 2.3$	0.199	$2.0 \pm 0.2 \pm 0.07$
0.071	$9.1 \pm 1.1 \pm 0.9$	0.285	$1.3 \pm 0.2 \pm 0.03$
0.100	$6.2 \pm 0.6 \pm 0.3$	0.456	$0.37 \pm 0.3 \pm 0.10$
0.142	$3.4 \pm 0.3 \pm 0.2$		

Table A7. Inclusive η spectrum at $\langle\sqrt{s}\rangle = 34.4$ GeV

$\langle x \rangle$	$s/\beta\,d\sigma/dx$(μb GeV^2)
0.047	$2.81 \pm 1.16 \pm 1.6$
0.071	$1.24 \pm 0.41 \pm 0.3$
0.181	$0.23 \pm 0.07 \pm 0.04$

References

1. JADE Collab., W. Bartel et al.: Phys. Lett. **88 B**, 171 (1979); Phys. Lett. **92 B**, 206 (1980); Phys. Lett. **99 B**, 277 (1981)
2. H. Drumm et al.: Nucl. Instrum. Methods **176**, 333 (1980)
3. E. Longo et al.: Nucl. Instrum. Methods **128**, 283 (1975)
4. B. Andersson, G. Gustafson, C. Peterson: Z. Phys. C - Particles and Fields **1**, 105 (1978); B. Andersson, G. Gustafson: Z. Phys. C - Particles and Fields **3**, 223 (1980); B. Andersson, G. Gustafson, T. Sjöstrand: Z. Phys. C - Particles and Fields **6**, 235 (1980); B. Andersson, G. Gustafson, T. Sjöstrand: Phys. Lett. **94 B**, 211 (1980)
5. F.A. Berends, R. Kleiss: Nucl. Phys. **B 178**, 141 (1981)
6. J. Kanzaki, S. Odaka: private communication
7. JADE Collab. W. Bartel et al.: Phys. Lett. **92 B**, 206 (1980)
8. JADE Collab. W. Bartel et al.: Phys. Lett. **101 B**, 129 (1981); Phys. Lett. **134 B**, 275 (1984); Z. Phys. C - Particles and Fields **21**, 37 (1983)
9. JADE Collab. W. Bartel et al.: Z. Phys. C - Particles and Fields **20**, 187 (1983)
10. TASSO Collab. M. Althoff et al.: Z. Phys. C - Particles and Fields **17**, 5 (1983)
11. CELLO Collab. H.J. Behrendt et al.: Z. Phys. C - Particles and Fields **20**, 207 (1983)
12. TASSO Collab. M. Althoff et al.: Z. Phys. C - Particles and Fields **22**, 307 (1984)
13. JADE Collab. W. Bartel et al.: Z. Phys. C - Particles and Fields **9**, 315 (1981)
14. D.L. Scharre et al.: Phys. Rev. Lett. **41**, 1005 (1978); CELLO Collab. H.J. Behrendt et al.: Z. Phys. C - Particles and Fields **14**, 189 (1982); PEP 4 Collab. H. Ahira et al.: Z. Phys. C - Particles and Fields **27**, 187 (1985)
15. TASSO Collab. W. Brandelik et al.: Phys. Lett. **108 B**, 71 (1982)
16. JADE Collab. W. Bartel et al.: Phys. Lett. **130 B**, 454 (1983)
17. E. Laermann et al.: Nucl. Phys. **B 207**, 205 (1982)
18. F.A. Berends, K.F. Gaemers, R. Gastmans: Nucl. Phys. **B 57**, 381 (1973); F.A. Berends, R. Kleiss: Nucl. Phys. **B 177**, 237 (1981)
19. T.F. Walsh, P.M. Zerwas: Phys. Lett. **44 B**, 195 (1973); S.J. Brodsky, C.E. Carlson, R. Suaya: Phys. Rev. **D 14**, 2264 (1973); K. Sazaki: Phys. Rev. **D 24**, 1177 (1981)
20. E. Fernandez et al.: Phys. Rev. Lett. **54**, 95 (1985)
21. Yung Su Tsai: SLAC-PUB-3129 (1983)